Nanostructure Analysis

DOI: 10.1002/anie.201001493

Imaging of Self-Assembled Structures: Interpretation of TEM and Cryo-TEM Images

*Heiner Friedrich, Peter M. Frederik, Gijsbertus de With, and Nico A. J. M. Sommerdijk**

cryogenic TEM · electron tomography · nanostructures · soft materials · transmission electron microscopy

The investigation of solution-borne nanostructures by transmission electron microscopy (TEM) is a frequently used analytical method in materials chemistry. In many cases, the preparation of the TEM sample involves drying and staining steps, and the collection of images leads to the interaction of the specimen with the electron beam. Both aspects call for cautious interpretation of the resulting electron micrographs. Alternatively, a near-native solvated state can be preserved by cryogenic vitrification and subsequent imaging by low-dose cryogenic TEM. In this Minireview, we provide a critical analysis of sample preparation, and more importantly, of the acquisition and interpretation of electron micrographs. This overview should provide a framework for the application of (cryo)-TEM as a powerful and reliable tool for the analysis of colloidal and self-assembled structures with nanoscopic dimensions.

1. Introduction

The fast-growing fields of nanotechnology and (macro)-molecular self-assembly have led to a strong and continuous demand for nanoscopic imaging of the resulting materials with nanometer detail. Whereas scanning-probe techniques, such as STM and AFM, have become the most important tools for the imaging of surface-associated structures, in the case of self-assembled and nanostructures in solution, transmission electron microscopy (TEM) is the technique of choice for the analysis of structure and morphology at the nanometer level. The widespread and frequent use of TEM as a characterization tool is illustrated in Figure 1, which shows that over 2500 TEM-based publications appeared in the first quarter of 2010 alone.[1]

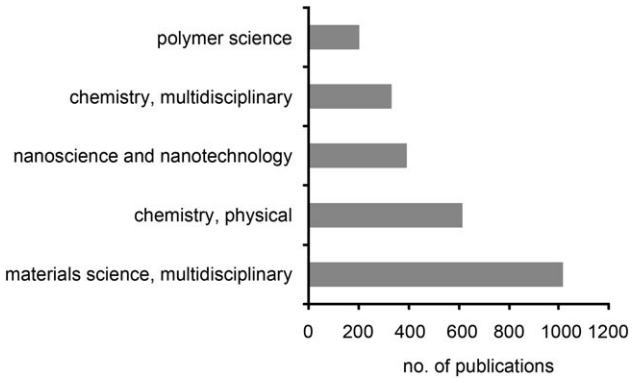

Figure 1. Data from the ISI Web of Science showing the importance of TEM in the different research areas: number of studies reported in the first quarter of 2010 in which TEM was used as a characterization tool.

Recent advances in TEM methodology and instrumentation have led to amazing new possibilities for the analysis of soft matter and self-assembled nanostructures. Moreover, the

[*] Dr. H. Friedrich, Dr. P. M. Frederik, Prof. Dr. G. de With, Dr. N. A. J. M. Sommerdijk
Department of Chemical Engineering and Chemistry
Laboratory of Materials and Interface Chemistry and
Soft Matter CryoTEM Research Unit
Eindhoven University of Technology
PO Box 513, 5600 MB Eindhoven (The Netherlands)
Fax: (+31) 40-245-1036
E-mail: n.sommerdijk@tue.nl
Homepage: http://www.cryotem.nl/

dissemination of these methods and their adoption by various scientific disciplines has significantly enhanced our understanding of how physical and chemical processes control the organization of matter across multiple length scales.[2] However, the availability of TEM to a large scientific community, in a similar manner to AFM, has also led to a increasing number of "nonexperts" becoming involved in the interpretation of micrographs of nanostructures. This phenomenon, and the fact that much of the available TEM methodology traditionally stems from either the biological or the (inorganic) materials sciences, frequently leads to the use of suboptimal processes for the preparation and treatment of the sample, as well as to the erroneous interpretation of the resulting images. With this Minireview, on the basis of our experience in the application of TEM in inorganic (H.F.), biological (P.M.F.), materials (G.d.W.), and supramolecular chemistry (N.A.J.M.S.), we hope to provide a guide for the preparation of TEM samples and, more importantly, for the interpretation of the micrographs obtained, but without urging the reader to use expensive and not readily accessible high-end equipment. Furthermore, we try to bridge the gap between the different scientific disciplines by encouraging the combination of TEM-based techniques that stem from seemingly unrelated fields.

2. Sample Preparation

For analysis with conventional TEM, as it has been used since the 1940s, solution-borne specimens are dried from a suspension onto a substrate: generally a 10–30 nm thick carbon or polymer film supported by a metal grid. In the case of organic materials, which are relatively translucent for the electron beam, drying is often combined with negative staining, which artificially enhances contrast for visualization of the structure and shape of the material under investigation.

2.1. Negative Staining

In this preparation method,[3] salt solutions of strongly electron scattering heavy-metal compounds, such as uranyl acetate, are added to the drying specimen to effectively form a mold of the specimen (Figure 2a,c).[4] Compositional differences and interfaces can be enhanced by selective interactions with the salt solution or with, for example, OsO_4 vapors.[5] Specimen preparation, in particular the grain size of the staining agent, generally precludes the sub-nanometer resolution that is routinely observed for robust inorganic specimens. Still, under optimal conditions, and depending on the precise experimental procedure, a resolution of 2 nm can be attained.[6]

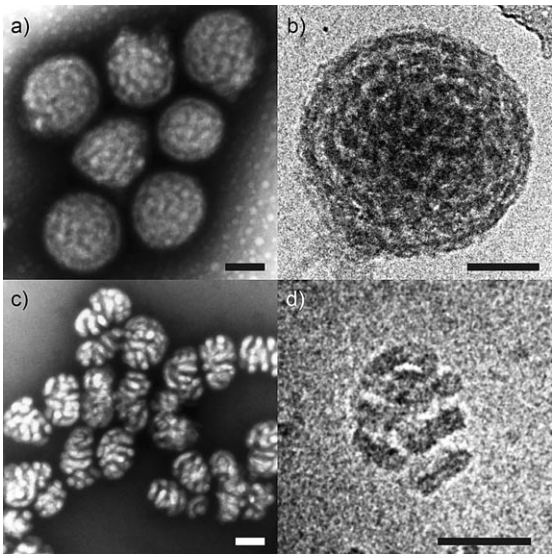

Figure 2. TEM imaging of aggregates of two peptide-based double-comb diblock copolymers (from Ref. [4]): a,c) negative staining with uranyl acetate; b,d) the respective cryogenic preparations (see also Figure 8). After negative staining, the density distribution in the image is dominated by the stain. The stain penetrates/reacts variably with the specimen; thus, the stain mold is not identical to the object. The cryo-TEM images represent the density distribution within the specimen. Although the density difference between the (negative) stain and the specimen is larger than the density difference between vitreous water and the specimen, the variation and uncertainty in stain penetration/reactivity makes the staining approach inferior when fine structural details have to be resolved. Scale bars are 100 nm.

These drying and staining procedures can affect the structure and morphology of the sample, and extreme care should be taken in the interpretation of the electron micrographs.[7] It is clear that the drying of solutions will dramatically change the concentration of the material and in many cases drive the self-assembly of solutes and aggregation of existing assemblies along nonequilibrium pathways. More precisely, the drying of suspended structures will expose them to the surface tension of the solvent, and the retracting liquid surface will sweep them into clusters. At the final stages of drying, the material is concentrated and pressed together, which can result in array formation (Figure 2a,c), the collapse of aggregate structures, and in some cases a stepwise (layer-by-layer) increase in sample thickness.[8]

In the case of aqueous samples, these effects can be counteracted by the addition of surface-active compounds or organic solvents, for example, methanol or ethanol;[9] however, these measures may themselves alter the structures under investigation. Also, freeze drying can be used to reduce

Nico A. J. M. Sommerdijk is Associate Professor of Materials and Interface Chemistry at the Eindhoven University of Technology. He completed his PhD in 1995 at the University of Nijmegen (Netherlands) in the field of organic and supramolecular chemistry. In 1999, after postdoctoral studies on inorganic materials and polymer self-assembly, he moved to Eindhoven University of Technology, where his research focuses on the use of cryo-TEM in the study of (macro)molecular assemblies and the use of these assemblies as templates for biomimetic mineralization.

the surface-tension effects associated with drying from solution, as well as to prevent the structural collapse that might occur upon removal of the solvent,[10] and leads to the deposition of the material that was originally dissolved in the solution. Furthermore, the interaction with staining agents may change both the nanostructure and morphology of the objects under investigation.[11]

2.2. Freeze–Fracture EM

Freeze–fracture electron microscopy (EM) can be used to avoid these artifacts.[12] This technique involves fast cooling of the sample by plunging it into liquid ethane or liquid propane. The temperature is maintained at approximately −160 °C while the frozen droplet is fractured with a cold "knife". The fracture path takes the route of lowest resistance and generally follows the contours of the nanostructures present at the fracture plane. These contours can be further accentuated through the sublimation of a thin layer of the ice; the features of the embedded objects then stand out more clearly.[13] An electron-transparent replica is prepared by evaporating a thin layer of carbon onto the fracture plane. The contrast needed to visualize the relief structure of the surface is generated by evaporating a metal, for example, platinum, onto the carbon film at an angle of approximately 45° ("shadowing"). Although elaborate, this technique has been shown to successfully reproduce amphiphilic nanostructures, such as vesicles and other bilayer aggregates.[14] However, its success depends primarily on the preference of the fracture plane to separate the two halves of the lipid bilayer to reveal information on the internal structure of the objects. In the absence of this effect, the replica can only reproduce the outer contours of the ice-embedded objects.

2.3. Plunge Freezing

With the introduction of cryogenic TEM (cryo-TEM), it became possible to image suspended organic material (Figure 2b,d).[15] Upon the plunge freezing of films approximately 100 nm thick of a (generally aqueous) solution into an appropriate coolant, such as liquid ethane at −183 °C, the nanostructures of interest become instantaneously embedded in an electron-transparent film of vitrified amorphous ice.[16] Through the use of phase-contrast imaging, which is discussed further in Section 4, the need for staining is overcome, and aqueous specimens can be studied in their near-native hydrated state. With state-of-the-art equipment, nanometer resolution is possible. Cryo-TEM also enables the imaging of non-aqueous solutions;[17] however, the conditions for sample preparation and image collection are more critical than for aqueous samples. During the vitrification process, the objects of interest remain in the suspending medium, and their mutual temporal and spatial arrangements are preserved. The vitrified specimen can subsequently be studied at temperatures low enough to avoid the recrystallization of the amorphous film. Nevertheless, several of the steps involved in the preparation of cryo-TEM samples may lead to the introduction of artifacts. The critical issues in these steps and the related potential pitfalls in the interpretation of the resulting micrographs are discussed in this and the following sections in more detail.

During sample preparation, a microliter drop of the sample is applied to a carrier grid and subsequently reduced about 5000 times in volume by blotting with filter paper to yield a thin film with a thickness of typically about 100 nm. The resulting thin film has a large surface-to-volume ratio that enables rapid heat exchange and ensures efficient vitrification. However, under ambient conditions, this surface-to-volume ratio also leads to rapid evaporation of the solvent with a concomitant significant increase in the sample concentration, a lowering of the temperature, and possibly a collapse of the embedded nanostructures (Figure 3).[18] For example, an evaporation rate of 40 nm s^{-1} from an aqueous film is expected under typical laboratory conditions (room temperature, 40% relative humidity): a dramatic rate for a 100 nm thick film. This effect of evaporation can only be prevented by working at close to 100% environmental humidity. Solvent saturation of the environment together with temperature control are thus essential for specimen preparation for cryo-TEM, and vitrification instruments have been developed to support these conditions. The most frequently used instruments are the Controlled Environment

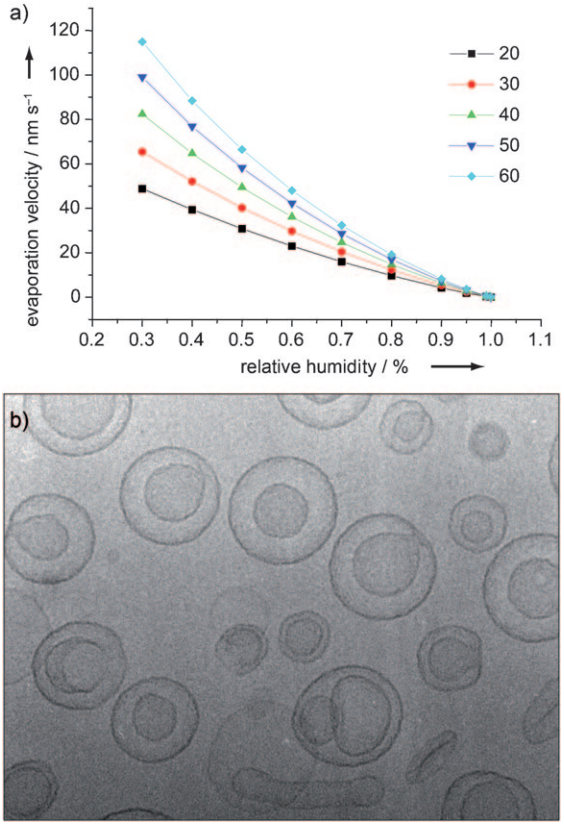

Figure 3. a) Rate of evaporation of a thin film subjected to several temperatures and environmental humidities. b) Osmotic collapse of spherical liposomes into "vaselike" structures (from Ref. [18]). Approximately 50% of the internal volume of the liposomes was lost during preparation at 25 °C and 40% relative humidity.

Vitrification System (CEVS) developed by Talmon and co-workers,[19] and the more advanced Vitrobot developed by Frederik and co-workers/FEI company.[20]

Other essential issues in the preparation of thin aqueous films are related to the sample support film. A good wettability of the support is needed for the formation of a thin continuous solvent film upon blotting with filter paper. For use with aqueous/polar solvents, this wettability is introduced by oxygen-plasma treatment (glow discharge).[21] Generally, amorphous-carbon support films with (circular) holes are used. On a wettable support, the applied liquid spreads out over the whole surface and has a slightly biconcave surface where it spans the holes. Consequently, the solvent film is thinner in the center of the holes than at the edges. This effect can lead to the sorting by size of the embedded nanostructures, with the smaller nanostructures located in the center of the holes, and the bigger nanostructures at the edges of the holes.[8]

The filter paper used for blotting should be inert; neither release of material from the filter paper nor the selective removal of sample components by the filter paper should occur. In our experience, the latter issue is a (poorly documented) point worthy of attention, in particular when aqueous dispersions of amphiphilic block copolymers are used. Moreover, the liquid flow induced by the blotting action of the filter paper may induce shear stress in the liquid and may thus lead to an orientation of the dispersed objects in the flow or in some cases even to morphological rearrangement of the self-assembled structures.[22] In these cases, a waiting time (seconds to minutes) should be applied between blotting and vitrification so that the film can relax and the original organization is again obtained.

The eventual vitrification of the thin film is achieved by shooting it with a velocity of typically 1.5–2 $m s^{-1}$ into a cooling medium with good heat-exchange properties, such as liquid ethane.[23] In the case of aqueous samples, when the cooling rate is too low, hexagonal ice is formed (Figures 4a and 5a), which hampers the reliable interpretation of the recorded images. Once vitrified, the specimen should be kept colder than 133 K to prevent devitrification of the film and its transformation into cubic ice (Figures 4b and 5b), which may be mistaken for embedded electron-dense particles belonging to the sample. The rapid cooling of liquid water or the slow deposition of water vapor on a cold surface leads to amorphous/vitreous ice (Figures 4c and 5c,d).

Another point of attention after vitrification is the protection of the specimen during transfer from the preparation chamber to the cryo-TEM sample holder, and subsequently into the microscope. During these stages, atmospheric water can deposit on the grid, generally as hexagonal ice, and appear as particulate material (Figure 5c,d). Again, it can thus interfere with the reliable interpretation of the images. Similarly, a porous layer of vitrified water can be deposited on the cold specimen if the partial vapor pressure of water in the high vacuum of the microscope column is too high (Figure 5e). It can be detected and removed by careful irradiation with a low-intensity electron beam (Figure 5e–h); care has to be taken not to affect the integrity of the underlying sample.

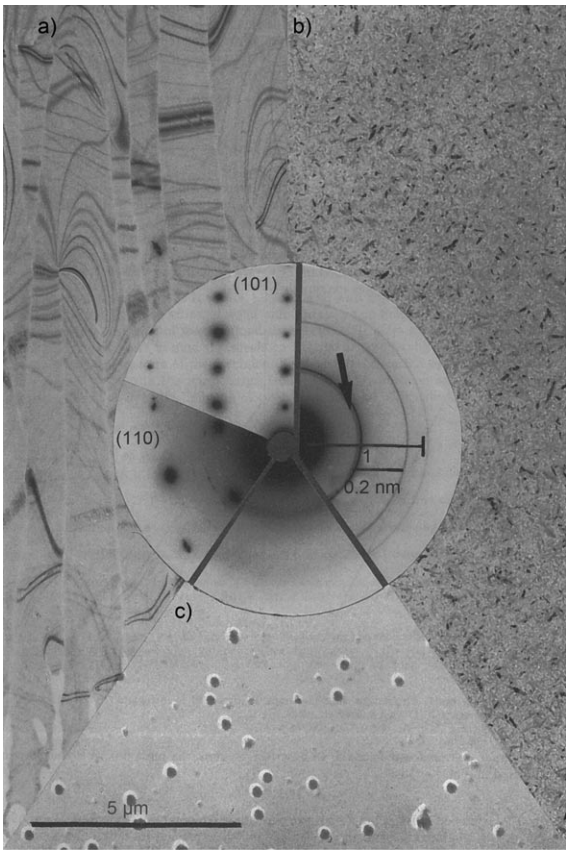

Figure 4. Cryo-TEM images and diffractograms of a) hexagonal ice, b) cubic ice, and c) vitreous ice and polystyrene spheres (from Ref. [16c]).

3. Low-Dose TEM and Cryo-TEM

One of the most important causes of artifacts and sometimes the misinterpretation of micrographs in TEM is electron-beam-induced radiation damage. All organic specimens, and under high magnification most inorganic specimens, suffer from degradation as a result of the impact of the high-energy electrons from the focused electron beam. The concomitant dissipation of energy gives rise to chemical reactions and rearrangements that lead to the loss of structural detail during image acquisition. In the case of organic materials, this behavior can also cause shrinkage and even the introduction of circular voids (Figure 5g), which are easily and frequently misinterpreted as the inner compartments of "vesicular structures". The fading and disappearance of diffraction spots as a function of dose is a measurable quantity for these destructive beam–specimen interactions.[24]

The damaging effect of electron irradiation can be reduced by lowering the specimen temperature, for example, by a factor of 3 to 6 between room temperature and liquid-nitrogen temperature.[25] Nevertheless, also in cryo-TEM samples, both the embedded nanostructures and the vitrified matrix (in particular for organic solvents) are sensitive to electron-beam-induced changes. The sensitivity depends on the composition of the specimen and even on the cooling velocity during specimen vitrification.[9] For this reason, low-

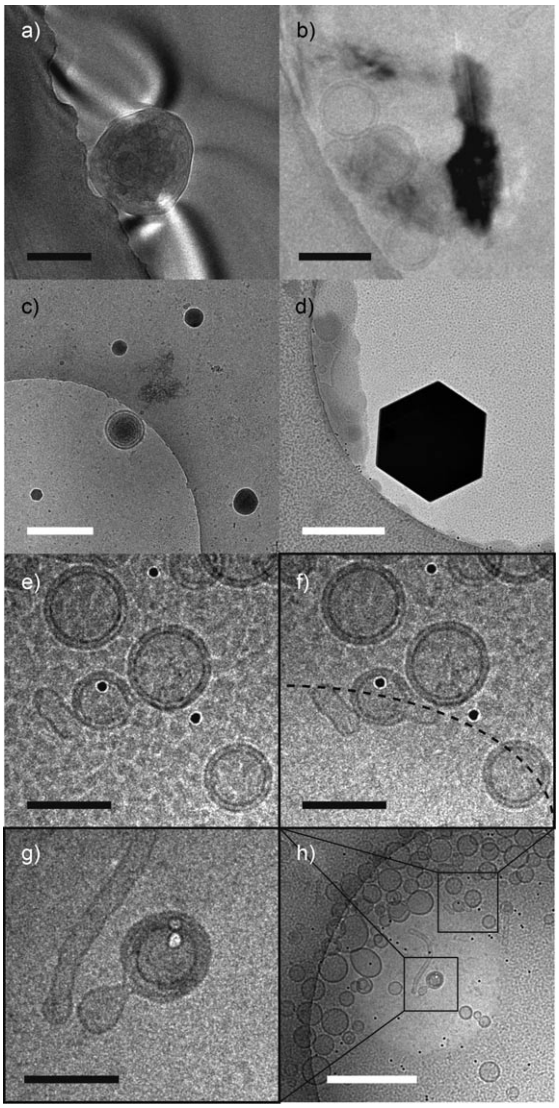

Figure 5. Cryo-TEM images of a) a polymer aggregate in hexagonal ice; b) lipid vesicles in cubic ice; c) a polymer aggregate (center) in vitreous ice and ice particulates; d) a hexagonal ice crystal on vitreous ice; e–h) ice contamination as a result of a high partial water vapor pressure in the microscope column, before (e) and after (f–h) irradiation. f) The dashed line indicates the border of the illuminated area. g) Lipid vesicle with a circular void as a result of beam damage. h) Low-magnification image; the irradiated area appears as a bright disk. Small dark spots are gold particles used for electron tomography. Black scale bars are 100 nm, and white scale bars are 500 nm.

dose techniques should be applied: a "safe" predetermined number of electrons per square nanometer should be used for each image so that the required information can be extracted before the specimen is damaged.

4. Image Contrast in (Cryo-)TEM

In TEM, two contrast mechanisms, amplitude and phase contrast, contribute to image formation. Amplitude contrast—scattering–absorption contrast related to density and atomic number—arises from the fact that some regions in the specimen scatter electrons more efficiently; therefore, fewer electrons are detected in the corresponding region of the image.[26] Phase contrast arises from the coherent interference of the scattered and transmitted beams. Defocusing of the image tunes the phase-contrast transfer function (CTF) to enhance or diminish a given structural detail of the specimen (Figure 6a).[27] Figure 6 also illustrates how the appearance and power spectrum of colloidal gold and silica particles on a carbon film change as the focus settings are varied. Conventionally, images are recorded with the electron beam focused below the plane of the specimen (negative focus values) to avoid contrast reversal (bright specimen on a dark support, as in Figure 6b). The directly interpretable resolution in an electron micrograph corresponds to the first zero crossing in the CTF and decreases with increasing defocus, as is best seen by the shift to lower frequencies (arrows in Figure 6a). For organic specimens, that is, specimens that are mainly composed of elements with low Z values, the contribution of amplitude contrast (related to density and atomic number) is so small that image formation relies exclusively on phase contrast up to dimensions of tens of nanometers.[28] It is therefore quite common to trade contrast for resolution and use large defocus settings in cryo-TEM. Furthermore, image contrast can be improved by zero-loss energy filtering, which decreases the blurring in images due to inelastically scattered electrons, for example, for thick or tilted (in tomography, see Section 5) specimens, but more importantly, for low-dose (cryogenic) specimens.[29]

In principle, phase-contrast imaging should be superior to X-ray and neutron diffraction[30] and annular dark-field scanning TEM[31] in terms of resolution for a given dose; however, experimentally the contrast is much lower than predicted by scattering physics.[32]

In rare instances, there is a near-perfect match between the vitrified matrix and the objects under investigation, and no contrast is observed even at extreme defocus settings. In this case, the object may be visualized by careful irradiation through selective beam damage (Figure 7).[33] For aqueous samples, contrast can also be modulated by increasing or decreasing the density of the vitrified matrix, for example, by adding glycerol or methanol to the solution, respectively.[9] Despite the changes that additives may induce in the samples under investigation,[11] cryo negative staining has shown promise in preserving the structure in some specimens to nanometer detail.[34] In cryo negative staining, the sample is embedded in a vitreous film containing a negative staining agent (e.g. ammonium molybdate). Under these conditions, the image contrast is increased significantly in comparison to that observed for native aqueous cryogenic preparations, so that lower defocus settings can be used during image acquisition, and the beam stability of the cryogenic specimen is also increased significantly.[34]

5. Three-Dimensional (Cryo)-TEM

The projection images yielded by (cryo)-TEM provide information on both the shape and the internal structure of

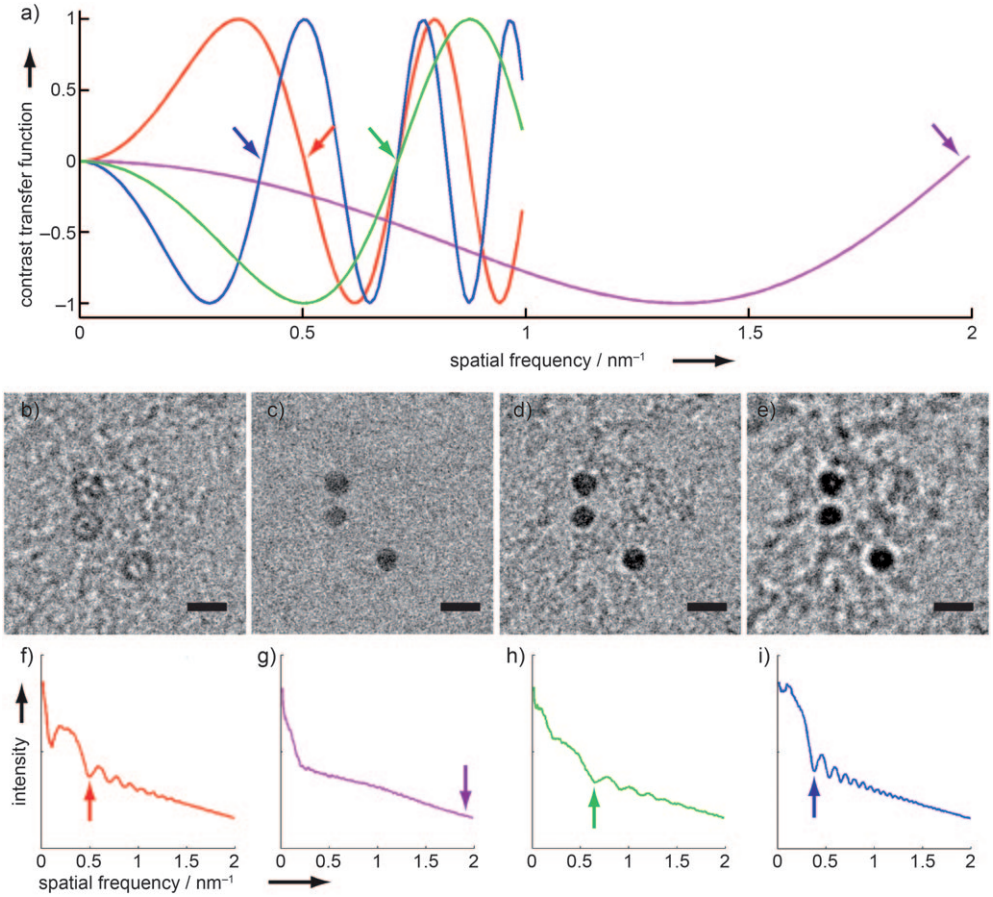

Figure 6. a) Contrast transfer function (of the cryoTITAN microscope at TU Eindhoven) calculated for defocus values of +2 μm (red), −150 nm (purple), −1 μm (green), and −3 μm (blue). The read, green, and blue curves are truncated at 1 nm^{-1} for better visibility. b–e) TEM images and f–i) power spectra of 10 nm colloidal gold (b,f) and 5 nm silica particles on a carbon support film with a defocus of +2 μm (b,f), −150 nm (c,g), −1 μm (d,h), and −3 μm (e,f). Scale bars are 10 nm. The silica particles formed agglomerates during drying on the support.

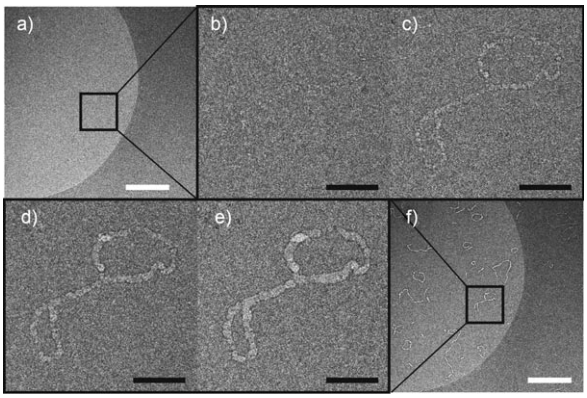

Figure 7. Cryo-TEM images of threadlike micelles of the amphiphilic triblock copolymer Pluronic 123 in a mixture of water and dimethylformamide. a,f) Low-magnification images (−40 μm defocus) before (a) and after (f) the induction of contrast by selective beam damage. b–e) Images showing the contrast increase with increasing electron dose (an increase of 3 $e^{-}A^{-2}$ per image at −5 μm defocus). White scale bars are 500 nm, and black scale bars are 100 nm.[51]

the nanostructures under investigation. One should, however, consider the effect of overlapping features in projections, similarly to the shadow play of a hand on a wall. The extension of imaging by TEM into three dimensions is possible by combining multiple projections from different directions.[35] At present, essentially two methodologies are available; the appropriate method is selected according to the degree of "structural uniqueness" of the sample.[35b] Both methods are employed for the analysis of self-assembled structures in cryogenic samples. If many structurally identical objects exist, powerful averaging methods (referred to as single-particle techniques) combine the information from multiple "copies" with multiple orientations into a single 3D reconstruction. Prominent examples are the 3D imaging of stacked bilayer helices formed by amphiphilic molecules and structurally persistent micelles.[36] In particular, a recent study on the micellar assembly of amphiphilic [3:3] hexakis adducts of C_{60} illustrates how single-particle techniques can resolve the internal organization of molecular aggregates of only 5 nm in size: the smallest persistent micelles detected so far.[36c]

For pleomorphic (unique) structures, as are generally present in synthetic samples, electron (cryo)tomography (ET)

is the technique of choice.[35,37] In (cryo-)ET, a large number of 2D projections are recorded from the same object at different angles and are combined to produce a 3D image. Our research group[4,38] and others[39] recently introduced the use of cryo-ET on synthetic hydrated specimens to reveal with nanometer detail the 3D organization of self-assembled structures. In these studies, in which a large series of images of the same area are recorded with different tilt angles, the use of low-dose techniques to prevent radiation damage is very important. Moreover, the processing of data in cryo-ET, from alignment to reconstruction to visualization, requires the utmost care on account of the low dose. Different 3D images obtained for a single sample through the use of different reconstruction and denoising algorithms are presented in Figure 8. Although reconstruction by weighted back projection followed by denoising is most common,[40] iterative[41] and discrete[42] approaches are gaining importance.

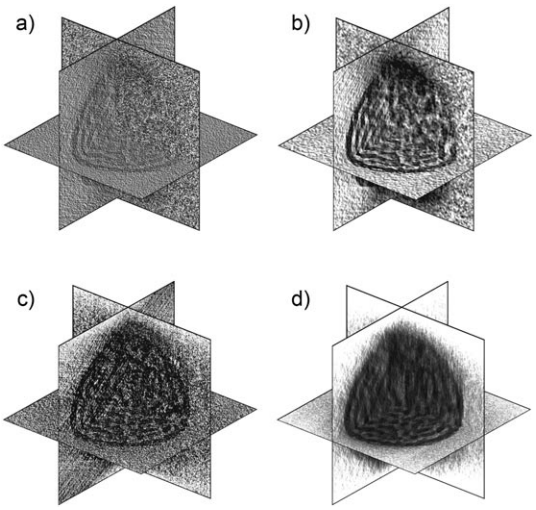

Figure 8. Bicontinuous aggregate of a peptide-based double-comb diblock copolymer visualized by using three perpendicular numerical cross-sections through reconstruction by: a) weighted back projection;[40b] b) weighted back projection and denoising;[40b,c] c) the algebraic reconstruction technique (ART)[41c] with three iterations; d) the sequential iterative reconstruction technique (SIRT)[41c] with 20 iterations (data taken from Ref. [4]).

6. Conclusions and Outlook

The recent advances in TEM methodology and instrumentation, and more importantly, their dissemination and adoption by various scientific disciplines, have led to a wealth of possibilities for the analysis of self-assembled nanostructures. Use of these analytical techniques has significantly enhanced our understanding of how physical and chemical processes control the organization of matter across multiple length scales.[2,37] A recent beautiful example[43] illustrates how far TEM has developed over the past few years: aberration-corrected TEM[44] with an acceleration voltage of only 80 kV provided atomic images of metal-mediated fullerene coalescence and nanotube rupture (Figure 9).[43] This and related developments bring us ever closer to characterizing chemical substances and reactions by "just looking" where the atoms are.[45]

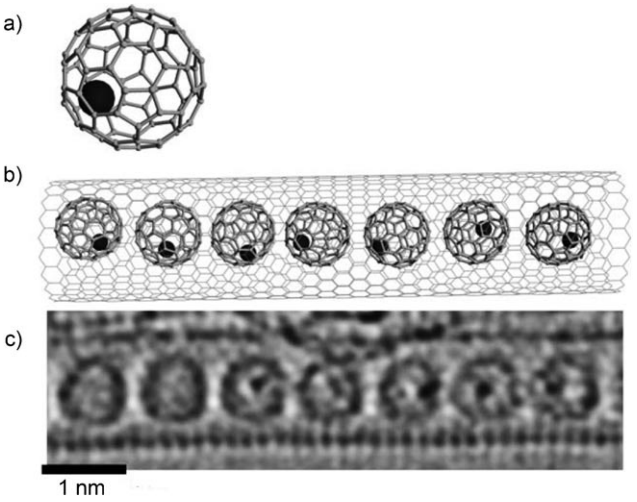

Figure 9. a) Model of a dysprosium atom encapsulated inside a C_{82} fullerene. b) Model of fullerenes aligned within a carbon nanotube. c) Aberration-corrected TEM image of dysprosium atoms inside C_{82} cages inside a nanotube (from Ref. [43]).

For the analysis of solution-borne nanostructures, and in particular self-organizing systems, the use of cryo-TEM is a growing field.[17,18,46] Remarkably, whereas electron cryotomography (cryo-ET, also referred to as 3D cryo-TEM) is currently developing into a major technique in life sciences,[47] its application in the study of nonbiological materials is virtually unexplored. Besides our cryo-ET studies on synthetic hydrated specimens,[4,38] our research group recently demonstrated the time-resolved cryo-TEM analysis of self-assembly and biomimetic mineralization processes.[38c,48] Within this approach, plunge freezing of the samples at different time points enabled the detailed analysis of all stages of the process under investigation with both 2D and 3D imaging as well as with diffraction techniques.

Nevertheless, we emphasize that although the quality of the TEM images may in part depend on the available equipment, it depends much more critically on the preparation of the sample and the imaging conditions. More importantly, the reliability of the conclusions drawn from the experiments fully depends on the careful interpretation of the data. Hence, complicated sample preparation and advanced imaging techniques may not be required if one can establish that the observed features are without doubt the result of the solution chemistry rather than of the procedures used to obtain the images.

Finally, the ability of TEM to provide detailed information on individual species inside a population is probably the strongest asset of the technique. However, it also brings about the greatest weakness: TEM may lead researchers to draw conclusions based on the observation of a limited number of objects and therefore should ideally be supported by information obtained for the entire population by collective approaches, such as scattering and spectroscopic techniques.[49] Nevertheless, we have high expectations from the latest developments in the field of TEM, in particular now

that 2D and 3D cryo-TEM methods can be combined with techniques such as scanning transmission electron microscopy (STEM), electron energy loss spectroscopy (EELS), and energy-dispersive X-ray spectroscopy (EDX), thereby effectively merging approaches that originate from the biological and materials sciences.[50]

We thank P. H. H. Bomans for his advice during the performance of cryo-TEM. This research is supported by the Dutch Polymer Institute (DPI) (grant number 688).

Received: March 12, 2010
Revised: April 19, 2010
Published online: September 6, 2010

[1] For selected studies reported in the first quarter of 2010 that illustrate the importance of TEM as a characterization tool in the field of (macromolecular) self-assembly and nanotechnology, see: a) F. Wang, Y. Han, C. S. Lim, Y. Lu, J. Wang, J. Xu, H. Chen, C. Zhang, M. Hong, X. Liu, *Nature* **2010**, *463*, 1061 – 1065; b) C. Kiely, *Nat. Mater.* **2010**, *9*, 296 – 297; c) C. Kisielowski, Q. M. Ramasse, L. P. Hansen, M. Brorson, A. Carlsson, A. M. Molenbroek, H. Topsøe, S. Helveg, *Angew. Chem.* **2010**, *122*, 2768 – 2770; *Angew. Chem. Int. Ed.* **2010**, *49*, 2708 – 2710; d) J. Bai, X. Zhong, S. Jiang, Y. Huang, X. Duan, *Nat. Nanotechnol.* **2010**, *5*, 190 – 194; e) D. S. Kim, Y. Yang, H. Kim, A. Berger, M. Knez, U. Gösele, V. Schmidt, *Angew. Chem.* **2010**, *122*, 215 – 218; *Angew. Chem. Int. Ed.* **2010**, *49*, 210 – 212; f) A. M. Caro, S. Armini, O. Richard, G. Maes, G. Borghs, C. M. Whelan, Y. Travaly, *Adv. Funct. Mater.* **2010**, *20*, 1125 – 1131; g) E. Bellido, R. de Miguel, D. Ruiz-Molina, A. Lostao, D. Maspoch, *Adv. Mater.* **2010**, *22*, 352 – 355; h) E. Pouget, N. Fay, E. Dujardin, N. Jamin, P. Berthault, L. Perrin, A. Pandit, T. Rose, C. Valéry, D. Thomas, M. Paternostre, F. Artzner, *J. Am. Chem. Soc.* **2010**, *132*, 4230 – 4241; i) M. A. Loi, J. Gao, F. Cordella, P. Blondeau, E. Menna, B. Bártová, C. Hébert, S. Lazar, G. A. Botton, M. Milko, C. Ambrosch-Draxl, *Adv. Mater.* **2010**, *22*, 1635 – 1639; j) R. Boldt, M. Kaiser, D. Kohler, F. Krumeich, M. Ruck, *Nano Lett.* **2010**, *10*, 208 – 210; k) Q. Chen, Y. Feng, D. Zhang, G. Zhang, Q. Fan, S. Sun, D. Zhu, *Adv. Funct. Mater.* **2010**, *20*, 36 – 42; l) A. J. Hong, C. C. Liu, Y. Wang, J. Kim, F. X. Xiu, S. X. Ji, J. Zou, P. F. Nealey, K. L. Wang, *Nano Lett.* **2010**, *10*, 224 – 229; m) C. C. Wang, L. H. Jimison, L. Goris, I. McCulloch, M. Heeney, A. Ziegler, A. Salleo, *Adv. Mater.* **2010**, *22*, 697 – 701; n) C. Vollmer, E. Redel, K. Abu-Shandi, R. Thomann, H. Manyar, C. Hardacre, C. Janiak, *Chem. Eur. J.* **2010**, *16*, 3849 – 3858; o) H. Yoshida, K. Kawamoto, H. Kubo, T. Tsuda, A. Fujii, S. Kuwabata, M. Ozaki, *Adv. Mater.* **2010**, *22*, 622 – 626; p) R. Chhabra, J. G. Moralez, J. Raez, T. Yamazaki, J. Y. Cho, A. J. Myles, A. Kovalenko, H. Fenniri, *J. Am. Chem. Soc.* **2010**, *132*, 32 – 33; q) X. Qi, C. Xue, X. Huang, Y. Huang, X. Zhou, H. Li, D. Liu, F. Boey, Q. Yan, W. Huang, S. De Feyter, K. Müllen, H. Zhang, *Adv. Funct. Mater.* **2010**, *20*, 43 – 49; r) H. Dong, F. Yan, H. Ji, D. K. Y. Wong, H. Ju, *Adv. Funct. Mater.* **2010**, *20*, 1173 – 1179; s) J. del Barrio, L. Oriol, C. Sanchez, J. L. Serrano, A. Di Cicco, P. Keller, M. H. Li, *J. Am. Chem. Soc.* **2010**, *132*, 3762 – 3769; t) S. Rehm, V. Stepanenko, X. Zhang, T. H. Rehm, F. Würthner, *Chem. Eur. J.* **2010**, *16*, 3372 – 3382; u) J. K. H. Hui, P. D. Frischmann, C.-H. Tso, C. A. Michal, M. J. MacLachlan, *Chem. Eur. J.* **2010**, *16*, 2453 – 2460; v) J. Voskuhl, M. C. A. Stuart, B. J. Ravoo, *Chem. Eur. J.* **2010**, *16*, 2790 – 2796; w) A. Bernecker, R. Wieneke, R. Riedel, M. Seibt, A. Geyer, C. Steinem, *J. Am. Chem. Soc.* **2010**, *132*, 1023 – 1031; x) H. R. Marsden, J. W. Handgraaf, F. Nudelman, N. Sommerdijk, A. Kros, *J. Am. Chem. Soc.* **2010**, *132*, 2370 – 2377; y) C. Sachse, N. Grigorieff, M. Fändrich, *Angew. Chem.* **2010**, *122*, 1343 – 1345; *Angew. Chem. Int. Ed.* **2010**, *49*, 1321 – 1323.

[2] S. Mann, *Nat. Mater.* **2009**, *8*, 781 – 792.

[3] a) S. Brenner, R. W. Horne, *Biochim. Biophys. Acta* **1959**, *34*, 103 – 110; b) A. D. Bangham, R. W. Horne, *J. Mol. Biol.* **1964**, *8*, 660 – 668; c) R. W. Horne, *Lab. Invest.* **1965**, *14*, 1054 – 1078.

[4] A. L. Parry, P. H. H. Bomans, S. J. Holder, N. A. J. M. Sommerdijk, S. C. G. Biagini, *Angew. Chem.* **2008**, *120*, 8991 – 8994; *Angew. Chem. Int. Ed.* **2008**, *47*, 8859 – 8862.

[5] a) H. R. Muller, *J. Ultrastruct. Res.* **1957**, *1*, 109 – 137; b) S. Bullivant, *Lab. Invest.* **1965**, *14*, 1178 – 1195; c) W. Stoeckenius, S. C. Mahr, *Lab. Invest.* **1965**, *14*, 1196 – 1207.

[6] a) A. Bremer, C. Henn, A. Engel, W. Baumeister, U. Aebi, *Ultramicroscopy* **1992**, *46*, 85 – 111; b) J. R. Harris, R. W. Horne, *Micron* **1994**, *25*, 5 – 13.

[7] Y. Talmon, *J. Colloid Interface Sci.* **1983**, *93*, 366 – 382.

[8] a) P. M. Frederik, M. C. A. Stuart, P. H. H. Bomans, W. M. Busing, *J. Microsc.* **1989**, *153*, 81 – 92; b) P. M. Frederik, M. C. A. Stuart, A. H. G. J. Schrijvers, P. H. H. Bomans, *Scanning Microsc.* **1989**, *Suppl. 3*, 277 – 284.

[9] a) P. M. Frederik, P. H. H. Bomans, M. C. A. Stuart, *Scanning Microsc.* **1991**, *Suppl. 5*, S43 – S52; b) P. M. Frederik, M. C. A. Stuart, P. H. H. Bomans, W. M. Busing, K. N. J. Burger, A. J. Verkleij, *J. Microsc.* **1991**, *161*, 253 – 262; c) P. M. Frederik, P. H. H. Bomans, M. C. A. Stuart, *Ultramicroscopy* **1993**, *48*, 107 – 119.

[10] R. W. G. Wyckoff, *Science* **1946**, *104*, 36 – 37.

[11] a) T. Kunitake, Y. Okahata, *J. Am. Chem. Soc.* **1977**, *99*, 3860 – 3861; b) C. Böttcher, C. Endisch, J.-H. Fuhrhop, C. Catterall, M. Eaton, *J. Am. Chem. Soc.* **1998**, *120*, 12 – 17.

[12] a) R. L. Steere, *J. Biophys. Biochem. Cytol.* **1957**, *3*, 45 – 60; b) H. Moor, K. Muhlethaler, *J. Cell Biol.* **1963**, *17*, 609; c) S. Bullivant, A. Ames, *J. Cell Biol.* **1966**, *29*, 435 – 447.

[13] D. W. Deamer, D. Branton, *Science* **1967**, *158*, 655 – 657.

[14] a) R. Vanvenetie, J. Leunissenbijvelt, A. J. Verkleij, P. H. J. T. Ververgaert, *J. Microsc.* **1980**, *118*, 401 – 408; b) R. A. Parente, M. Hochli, B. R. Lentz, *Biochim. Biophys. Acta Biomembr.* **1985**, *812*, 493 – 502; c) J. P. P. Starink, A. J. Verkleij, *J. Microsc.* **1992**, *167*, 181 – 196; d) N. Skalko, J. Bouwstra, F. Spies, M. Stuart, P. M. Frederik, G. Gregoriadis, *Biochim. Biophys. Acta Biomembr.* **1998**, *1370*, 151 – 160.

[15] K. A. Taylor, R. M. Glaeser, *Science* **1974**, *186*, 1036 – 1037.

[16] a) J. Dubochet, A. W. McDowall, *J. Microsc.* **1981**, *124*, Rp3 – Rp4; b) J. Dubochet, J. J. Chang, R. Freeman, J. Lepault, A. W. McDowall, *Ultramicroscopy* **1982**, *10*, 55 – 61; c) J. Dubochet, J. Lepault, R. Freeman, J. A. Berriman, J. C. Homo, *J. Microsc.* **1982**, *128*, 219 – 237.

[17] See, for example: a) G. T. Oostergetel, F. J. Esselink, G. Hadziioannou, *Langmuir* **1995**, *11*, 3721 – 3724; b) C. Boettcher, B. Schade, J.-H. Fuhrhop, *Langmuir* **2001**, *17*, 873 – 877; c) K. Butter, P. H. Bomans, P. M. Frederik, G. J. Vroege, A. P. Philipse, *J. Phys. Condens. Matter* **2003**, *15*, S1451 – S1470; d) H. Cui, T. K. Hodgdon, E. W. Kaler, L. Abezgauz, D. Danino, M. Lubovsky, Y. Talmon, D. J. Pochan, *Soft Matter* **2007**, *3*, 945 – 955; e) J. van Herrikhuyzen, S. J. George, M. R. J. Vos, N. A. J. M. Sommerdijk, A. Ajayaghosh, R. A. J. Janssen, E. W. Meijer, S. C. J. Meskers, A. P. H. Schenning, *Angew. Chem.* **2007**, *119*, 1857 – 1860; *Angew. Chem. Int. Ed.* **2007**, *46*, 1825 – 1828.

[18] P. M. Frederik, D. H. W. Hubert, *Liposomes Part E* **2005**, *391*, 431 – 448.

[19] J. R. Bellare, H. T. Davis, L. E. Scriven, Y. Talmon, *J. Electron Microsc. Tech.* **1988**, *10*, 87 – 111.

[20] M. R. Vos, P. H. H. Bomans, P. M. Frederik, N. A. J. M. Sommerdijk, *Ultramicroscopy* **2008**, *108*, 1478 – 1483.

[21] K. A. Taylor, R. M. Glaeser, *Rev. Sci. Instrum.* **1973**, *44*, 1546 – 1547.

[22] Y. Zheng, Z. Lin, J. L. Zakin, Y. Talmon, H. T. Davis, L. E. Scriven, *J. Phys. Chem. B* **2000**, *104*, 5263 – 5271.
[23] For many samples in organic media, liquid ethane is a good solvent, and liquid nitrogen might be the coolant of choice (see also Table 2 in Ref. [17d]).
[24] a) R. M. Glaeser, *J. Ultrastruct. Res.* **1971**, *36*, 466 – 482; b) S. M. Salih, V. E. Cosslett, *Philos. Mag.* **1974**, *30*, 225 – 228; c) R. M. Glaeser, *J. Struct. Biol.* **2008**, *163*, 271 – 276.
[25] W. Chiu, K. H. Downing, J. Dubochet, R. M. Glaeser, H. G. Heide, E. Knapek, D. A. Kopf, M. K. Lamvik, J. Lepault, J. D. Robertson, E. Zeitler, F. Zemlin, *J. Microsc.* **1986**, *141*, 385 – 391.
[26] R. Eusemann, H. Rose, J. Dubochet, *J. Microsc.* **1982**, *128*, 239 – 249.
[27] a) L. Reimer, *Transmission Electron Microscopy*, 4th ed., Springer, Berlin, **1997**; b) D. B. Williams, C. B. Carter, *Transmission Electron Microscopy: A Textbook for Materials Science*, 2nd ed., Springer, Berlin, **2009**.
[28] J. Dubochet, M. Adrian, J. J. Chang, J. C. Homo, J. Lepault, A. W. McDowall, P. Schultz, *Q. Rev. Biophys.* **1988**, *21*, 129 – 228.
[29] R. Grimm, D. Typke, W. Baumeister, *J. Microsc.* **1998**, *190*, 339 – 349.
[30] R. Henderson, *Q. Rev. Biophys.* **1995**, *28*, 171 – 193.
[31] P. Rez, *Ultramicroscopy* **2003**, *96*, 117 – 124.
[32] a) R. Henderson, R. M. Glaeser, *Ultramicroscopy* **1985**, *16*, 139 – 150; b) D. Typke, K. H. Downing, R. M. Glaeser, *Microsc. Microanal.* **2004**, *10*, 21 – 27.
[33] a) K. Mortensen, Y. Talmon, *Macromolecules* **1995**, *28*, 8829 – 8834; b) Y. Yan, H. Hoffmann, A. Makarsky, W. Richter, Y. Talmon, *J. Phys. Chem. B* **2007**, *111*, 6374 – 6382.
[34] a) M. Adrian, J. Dubochet, S. D. Fuller, J. R. Harris, *Micron* **1998**, *29*, 145 – 160; b) H. Stahlberg, E. Kutejova, K. Suda, B. Wolpensinger, A. Lustig, G. Schatz, A. Engel, C. K. Suzuki, *Proc. Natl. Acad. Sci. USA* **1999**, *96*, 6787 – 6790; c) S. De Carlo, C. El-Bez, C. Alvarez-Rúa, J. Borge, J. Dubochet, *J. Struct. Biol.* **2002**, *138*, 216 – 226.
[35] a) *Electron Tomography: Methods for the Three-Dimensional Visualization of Structures in the Cell*, 2nd ed. (Ed.: J. Frank), Springer Science + Business Media, LLC, New York, **2006**; b) *Three-Dimensional Electron Microscopy of Macromolecular Assemblies*, 2nd ed. (Ed.: J. Frank), Oxford University Press, New York, **2006**; c) *Advanced Tomographic Methods in Materials Research and Engineering* (Ed.: J. Banhard), Oxford University Press, New York, **2008**.
[36] a) C. Böttcher, H. Stark, M. van Heel, *Ultramicroscopy* **1996**, *62*, 133 – 139; b) M. Kellermann, W. Bauer, A. Hirsch, B. Schade, K. Ludwig, C. Böttcher, *Angew. Chem.* **2004**, *116*, 3019 – 3022; *Angew. Chem. Int. Ed.* **2004**, *43*, 2959 – 2962; c) B. Schade, K. Ludwig, C. Böttcher, U. Hartnagel, A. Hirsch, *Angew. Chem.* **2007**, *119*, 4472 – 4475; *Angew. Chem. Int. Ed.* **2007**, *46*, 4393 – 4396.
[37] See, for example: a) H. Friedrich, P. E. de Jongh, A. J. Verkleij, K. P. de Jong, *Chem. Rev.* **2009**, *109*, 1613 – 1629; b) P. A. Midgley, R. E. Dunin-Borkowski, *Nat. Mater.* **2009**, *8*, 271 – 280; c) H. Friedrich, C. J. Gommes, K. Overgaag, J. D. Meeldijk, W. H. Evers, B. de Nijs, M. P. Boneschanscher, P. E. de Jongh, A. J. Verkleij, K. P. de Jong, A. van Blaaderen, D. Vanmaekelbergh, *Nano Lett.* **2009**, *9*, 2719 – 2724.
[38] a) M. R. J. Vos, P. H. H. Bomans, F. de Haas, P. M. Frederik, J. A. Jansen, R. J. M. Nolte, N. A. J. M. Sommerdijk, *J. Am. Chem. Soc.* **2007**, *129*, 11894 – 11895; b) M. R. J. Vos, M. Breurken, P. E. L. G. Leclere, P. H. H. Bomans, F. de Haas, P. M. Frederik, J. A. Jansen, R. J. M. Nolte, N. A. J. M. Sommerdijk, *J. Am. Chem. Soc.* **2008**, *130*, 12608 – 12609; c) E. M. Pouget, P. H. H. Bomans, J. A. C. M. Goos, P. M. Frederik, G. de With, N. A. J. M. Sommerdijk, *Science* **2009**, *323*, 1455 – 1458; d) T. M. Hermans, M. A. C. Broeren, N. Gomopoulos, P. van der Schoot, M. H. P. van Genderen, N. A. J. M. Sommerdijk, G. Fytas, E. W. Meijer, *Nat. Nanotechnol.* **2009**, *4*, 721 – 726; e) H. M. H. F. Sanders, G. J. Strijkers, W. J. M. Mulder, H. R. Huinink, S. J. F. Erich, O. C. G. Adan, N. A. J. M. Sommerdijk, M. Merkx, K. Nicolay, *Contrast Media Mol. Imaging* **2009**, *4*, 81 – 88; f) B. Leng, Z. Shao, P. H. H. Bomans, L. J. Brylka, N. A. J. M. Sommerdijk, G. de With, W. Ming, *Chem. Commun.* **2010**, *46*, 1703 – 1705.
[39] a) Y. Chen, J. Du, M. Xiong, H. Guo, H. Jinnai, T. Kaneko, *Macromolecules* **2007**, *40*, 4389 – 4392; b) H. v. Berlepsch, C. Böttcher, K. Skrabania, A. Laschewsky, *Chem. Commun.* **2009**, 2290 – 2292.
[40] a) M. Radermacher in *Electron Tomography: Methods for the Three-Dimensional Visualization of Structures in the Cell*, 2nd ed. (Ed.: J. Frank), Springer Science + Business Media, LLC, New York, **2006**, pp. 245 – 274; b) J. R. Kremer, D. N. Mastronarde, J. R. McIntosh, *J. Struct. Biol.* **1996**, *116*, 71 – 76; c) A. S. Frangakis, R. Hegerl, *J. Struct. Biol.* **2001**, *135*, 239 – 250.
[41] a) P. A. Midgley, M. Weyland, *Ultramicroscopy* **2003**, *96*, 413 – 431; b) J. Tong, I. Arslan, P. Midgley, *J. Struct. Biol.* **2006**, *153*, 55 – 63; c) Inspect3D (FEI company, Eindhoven, The Netherlands).
[42] K. J. Batenburg, S. Bals, J. Sijbers, C. Kubel, P. A. Midgley, J. C. Hernandez, U. Kaiser, E. R. Encina, E. A. Coronado, G. Van Tendeloo, *Ultramicroscopy* **2009**, *109*, 730 – 740.
[43] A. Chuvilin, A. N. Khlobystov, D. Obergfell, M. Haluska, S. Yang, S. Roth, U. Kaiser, *Angew. Chem.* **2010**, *122*, 197 – 201; *Angew. Chem. Int. Ed.* **2010**, *49*, 193 – 196.
[44] a) M. Haider, H. Rose, S. Uhlemann, B. Kabius, K. Urban, *J. Electron Microsc.* **1998**, *47*, 395 – 405; b) D. J. Smith, *Microsc. Microanal.* **2008**, *14*, 2 – 15; c) M. Haider, P. Hartel, H. Muller, S. Uhlemann, J. Zach, *Philos. Trans. R. Soc. London Ser. A* **2009**, *367*, 3665 – 3682.
[45] R. P. Feynman, *Caltech J. Eng.Sci.* **1960**, *4*, 23 – 36.
[46] a) K. Butter, P. H. H. Bomans, P. M. Frederik, G. J. Vroege, A. P. Philipse, *Nat. Mater.* **2003**, *2*, 88 – 91; b) Y. Y. Won, *Korean J. Chem. Eng.* **2004**, *21*, 296 – 302; c) M. Klokkenburg, A. J. Houtepen, R. Koole, J. W. J. de Folter, B. H. Erne, E. van Faassen, D. Vanmaekelbergh, *Nano Lett.* **2007**, *7*, 2931 – 2936; d) V. M. Yuwono, N. D. Burrows, J. A. Soltis, R. L. Penn, *J. Am. Chem. Soc.* **2010**, *132*, 2163 – 2165.
[47] a) R. McIntosh, D. Nicastro, D. Mastronarde, *Trends Cell Biol.* **2005**, *15*, 43 – 51; b) A. J. Koster, M. Barcena in *Electron Tomography: Methods for the Three-Dimensional Visualization of Structures in the Cell*, 2nd ed. (Ed.: J. Frank), Springer Science + Business Media, LLC, New York, **2006**, pp. 113 – 162; c) S. Nickell, C. Kofler, A. P. Leis, W. Baumeister, *Nat. Rev. Mol. Cell Biol.* **2006**, *7*, 225 – 230.
[48] B. P. Pichon, P. H. H. Bomans, P. M. Frederik, N. A. J. M. Sommerdijk, *J. Am. Chem. Soc.* **2008**, *130*, 4034 – 4040.
[49] a) O. Regev, Y. Cohen, E. Kehat, Y. Talmon, *Zeolites* **1994**, *14*, 314 – 319; b) S. Bucak, C. Cenker, I. Nasir, U. Olsson, M. Zackrisson, *Langmuir* **2009**, *25*, 4262 – 4265; c) C. J. Gommes, H. Friedrich, P. E. de Jongh, K. P. de Jong, *Acta Mater.* **2010**, *58*, 770 – 780.
[50] A. Dey, G. de With, N. A. J. M. Sommerdijk, *Chem. Soc. Rev.* **2010**, *39*, 397 – 409.
[51] A. G. Denkova, P. H. H. Bomans, N. A. J. M. Sommerdijk, E Mendes, unpublished results.

